Application of Different Hill's Yield Criteria to Predict Limit Strains for Aerospace Titanium and Aluminum Sheet Alloys

M. Janbakhsh*
Center of Applied Science and Technology,
Jame Eslami Kargaran, Esfahan, Iran
E-mail: milad.janbakhsh@gmail.com
*Corresponding author

S. M. R. Loghmanian
Department of Engineering,
Islamic Azad University, Mobarakeh Branch, Iran
E-mail: m.loghmaniam@mau.ac.ir

F. Djavanroodi
College of Engineering, Qassim University, Saudi Arabia
E-mail: roodi@qec.edu.sa

Abstract: More recently, titanium and aluminum alloys are gaining more interests to be implemented in hydro-forming applications. It is necessary to predict forming limits for these sheet alloys. Forming limits play an important role in metal forming processes. Forming limit diagrams, present the limit strains for various linear strain paths. In other hand, forming limit curve (FLC), illustrates localized formability for sheet metals under proportional loadings and are known as a powerful tool for trouble-shooting in sheet metal forming processes. In this study, mechanical properties of Ti-6Al-4V titanium sheets, AA7075-T6 and AA2024-T3 aluminum sheets are investigated through the uni-axial tensile test. Anisotropy coefficients as well as work-hardening exponent resulted from tensile test were used to theoretical prediction and numerical simulation of limit strains. For the theoretical prediction of the forming limit curves, several constitutive models were implemented. Several Hill's yield criteria combined with Swift equation and empirical equation proposed by NADDRG were accomplished to predict the FLDs. Results showed that calculated numerical results are in good agreement with the predicted theoretical data when Hill93-Swift is the used instability criteria.

Keywords: Anisotropy, Forming Limit Diagram, Hill-Swift, Tensile Test, Strain path

Biographical notes: M. Janbakhsh has MSc degree in mechanical engineering from Iran University of Science and Technology and is now studying for PhD in Amirkabir University of Technology. His field of research is about biaxial flow stress and FLDs of titanium and aluminum sheet alloys. **S. M. R. Loghmanian** is an assistant professor in engineering department of Islamic Azad University, Mobarakeh branch. **F. Djavanroodi** is an assistant professor in mechanical engineering department in Iran University of Science and Technology. His field of interest is metal forming and Finite Element Method.

1   INTRODUCTION

Due to increasing demands for light weighting of components used in aerospace and automotive industries, recently, titanium sheet alloys are gaining special interests in production of structural parts. Regarding to combination of high strength to weight ratio with good cold formability along with corrosion resistance, titanium alloys have made improvements in structural parts of spaceflights.

For better understanding of cold formability of titanium sheet alloys, their behavior under sheet metal forming operations must be determined both experimentally and theoretically. Sheet metal formability is often evaluated by the practical concept called forming limit diagram (FLD). This concept is used to determine how close the sheet metal is to tearing and fracture under sheet metal forming operations such as stampings, hydro-forming and etc.

The concept of FLD was first introduced by Keeler [1] and Goodwin [2]. Pursuing the proposed diagram, many theoretical attempts have been made to predict sheet metal formability. Hill's localized instability criterion [3] combined with Swift's diffused instability criterion [4] was the first analytical approach to predict FLDs. This approach showed that both sides of forming limit curves (FLCs), are influenced by material parameters such as work hardening exponent and anisotropy coefficient. Several investigations [5-18] have been carried out with this analytical approach. The so-called M-K model [13] was developed by Marciniak and Kuczynski.

This model as well as Hill-Swift theory has gained increasing interests for decades. Although against Hill-Swift theory, in M-K analysis, the strain rate sensitivity factor (m) is considered, there are still some limitations for M-K analysis. The M-K model has brought out based on the assumption of an initial defect in perpendicular direction with respect to loading direction. The assumption made for this non-homogeneity factor is subjective and the forming limit diagram is directly influenced by it.

The objective of the present study is to establish a framework to analysis of formability of Ti-6Al-4V titanium sheet and AA7075-T6 and AA2024-T3 aluminum alloy when submitted to linear strain path. The detailed objectives are to:

1) Theoretically prediction of forming limit diagram for Ti-6Al-4V, AA7075-T6 and AA2024-T3 sheets by using different analytical models.

2) Investigate factors which significantly influence the FLD.

3) Compare numerical and theoretical results to discern which theoretical criterion is in better agreement with the numerical approach.

2   THEORETICAL BACKGROUND

Yield criteria define a relationship between stress components when yielding occurs. This is highly applicable to use yield locus when numerically analyzing the behavior of sheet material under deformation processes. Eq. (1) expresses an overall form of plastic flow behavior of sheet material.

$$F(\sigma_1, \sigma_2, \sigma_3, Y) = 0 \tag{1}$$

For an ideal isotropic material, yield criteria such as maximum shear stress criterion as well as strain energy criterion are the most applicable.

2.1. Von-Mises yield criterion
For an ideal case of isotropic material, the Von-Mises yield criterion can be written as in Eq. (2).

$$\sigma_1^2 + \sigma_2^2 - \sigma_1\sigma_2 + 3\sigma_{12}^2 = \sigma_{YF} \tag{2}$$

2.2. Hill's yield criteria
Since sheet metal is influenced by rolling conditions when manufactured and also mechanical properties of rolled sheets vary from each direction (with respect to rolling direction) to another direction, Hill introduced a yield criterion considering anisotropy of the sheet material [14].

$$2f(\sigma_{ij}) = F(\sigma_y - \sigma_z)^2 + G(\sigma_z - \sigma_x)^2 + H(\sigma_x - \sigma_y)^2 +$$
$$2L\tau_{yz}^2 + 2M\tau_{zx}^2 + 2N\tau_{xy}^2 = 1 \tag{3}$$

In Eq. (3), f is the yield function and F, G, H, L, M and N denote the material constants and are obtained from anisotropy coefficients deduced from uni-axial tensile test while x, y and z are the anisotropy axes. Material constants can be expressed in terms of six yield stress ratios r_{11}, r_{22}, r_{33}, r_{12}, r_{13} and r_{23} according to Eqs. (4) and (5).

$$F = \frac{1}{2}\left(\frac{1}{r_{22}^2} + \frac{1}{r_{33}^2} - \frac{1}{r_{11}^2}\right)$$

$$G = \frac{1}{2}\left(\frac{1}{r_{11}^2} + \frac{1}{r_{33}^2} - \frac{1}{r_{22}^2}\right)$$

(4)

$$H = \frac{1}{2}\left(\frac{1}{r_{11}^2} + \frac{1}{r_{22}^2} - \frac{1}{r_{33}^2}\right)$$

$$L = \frac{3}{2r_{23}^2}, \qquad M = \frac{3}{2r_{13}^2}, \qquad N = \frac{3}{2r_{12}^2}$$

$$r_{11} = r_{13} = r_{23} = 1, \qquad r_{22} = \sqrt{\frac{R_{90}(R_0+1)}{R_0(R_{90}+1)}}$$

(5)

$$r_{33} = \sqrt{\frac{R_{90}(R_0+1)}{R_{90}+R_0}}, \qquad r_{12} = \sqrt{\frac{3R_{90}(R_0+1)}{(2R_{45}+1)(R_{90}+R_0)}},$$

In sheet metal forming operations, it is assumed that thickness stress in comparison with two orthogonal stress components is insignificant. Therefore, thickness stress is eliminated from Eq. (3) and by making the assumption that anisotropy directions are the principal directions ($\sigma_x = \sigma_1, \sigma_y = \sigma_2, \tau_{xy} = o$), Hill's 48 yield criterion can be simplified to Eq. (6).

$$\sigma_1^2 - \frac{2R_o}{1+R_0}\sigma_1\sigma_2 + \frac{R_0(1+R_{90})}{R_{90}(1+R_0)}\sigma_2^2 = \sigma_0^2$$

(6)

The user-friendly Hill'93 yield criterion which was suitable for expressing the behavior of thin sheet metals under deformation processes was proposed in Ref. [15] as in Eqs. (7) and (8).

$$\frac{\sigma_1^2}{\sigma_0^2} - \frac{c\sigma_1\sigma_2}{\sigma_0\sigma_{90}} + \frac{\sigma_2^2}{\sigma_{90}^2} + \left[(p+q) - \frac{(p\sigma_1+q\sigma_2)}{\sigma_b}\right]\frac{\sigma_1\sigma_2}{\sigma_0\sigma_{90}} = 1 \quad (7)$$

Where

$$\frac{c}{\sigma_0\sigma_{90}} = \frac{1}{\sigma_0^2} + \frac{1}{\sigma_{90}^2} - \frac{1}{\sigma_b^2}$$

(8)

$$p = \left[\frac{2R_0(\sigma_b-\sigma_{90})}{(1+R_0)\sigma_0^2} - \frac{2R_{90}\sigma_b}{(1+R_{90})\sigma_{90}^2} + \frac{c}{\sigma_0}\right]\frac{1}{\frac{1}{\sigma_0} + \frac{1}{\sigma_{90}} - \frac{1}{\sigma_b}}$$

$$q = \left[\frac{2R_{90}(\sigma_b-\sigma_0)}{(1+R_{90})\sigma_{90}^2} - \frac{2R_0\sigma_b}{(1+R_0)\sigma_0^2} + \frac{c}{\sigma_{90}}\right]\frac{1}{\frac{1}{\sigma_0} + \frac{1}{\sigma_{90}} - \frac{1}{\sigma_b}}$$

2.3. Analytical models for calculation of FLD
2.3.1. Swift models with different Hill's yield criteria
Swift [4] used an equation to determine the limit strains in right side of the FLD (positive minor strain range). By making the assumption that the material follows the work-hardening law, Swift presented the limit strains as shown in Eq. (9).

$$\varepsilon_1^* = \frac{\sigma_1\left(\frac{\partial f}{\partial\sigma_1}\right)^2 + \sigma_2\left(\frac{\partial f}{\partial\sigma_2}\right)\left(\frac{\partial f}{\partial\sigma_1}\right)}{\sigma_1\left(\frac{\partial f}{\partial\sigma_1}\right)^2 + \sigma_2\left(\frac{\partial f}{\partial\sigma_2}\right)^2}$$

(9)

$$\varepsilon_2^* = \frac{\sigma_2\left(\frac{\partial f}{\partial\sigma_1}\right)^2 + \sigma_1\left(\frac{\partial f}{\partial\sigma_1}\right)\left(\frac{\partial f}{\partial\sigma_2}\right)}{\sigma_1\left(\frac{\partial f}{\partial\sigma_1}\right)^2 + \sigma_2\left(\frac{\partial f}{\partial\sigma_2}\right)^2}$$

By implementing the Swift equations and using Hill's 48 yield function, limit strains as a function of stress ratio (α) and material parameters (work-hardening exponent and anisotropy coefficients) are obtained as in Eqs. (10) and (11).

$$\frac{\partial f}{\partial\sigma_1} = \left(2 - \frac{2R_0}{1+R_0}\alpha\right)\sigma_1$$

(10)

$$\frac{\partial f}{\partial\sigma_2} = \left(2\alpha\frac{R_0(1+R_{90})}{R_{90}(1+R_0)} - \frac{2R_0}{1+R_0}\right)\sigma_1$$

$$\varepsilon_1^* = \frac{(1+R_0-R_0\alpha)\left[1+R_0+\alpha^2\left(\frac{R_0}{R_{90}}\right)(1+R_{90})-2\alpha R_0\right]}{(1+R_0-R_0\alpha)^2 + \alpha\left(\alpha\frac{R_0(1+R_{90})}{R_{90}}-R_0\right)^2}n$$

(11)

$$\varepsilon_2^* = \frac{(1+R_0-R_0\alpha)\left[\alpha+\alpha R_0+\alpha^2 R_0+\alpha\left(\frac{R_0}{R_{90}}\right)(1+R_{90})-R_0\right]}{(1+R_0-R_0\alpha)^2 + \alpha\left(\alpha\frac{R_0(1+R_{90})}{R_{90}}-R_0\right)^2}n$$

By taking into account the Hill's 93 yield function and implementing Swift equation, as represented in Eqs. (12) and (13), Banabic represented an approach to calculate the right side of the FLD [16].

$$\frac{\partial f}{\partial \sigma_1} = r = 2\sigma_{90}^2 + \alpha\sigma_0\sigma_{90}[c + p + q - (pt + q\alpha t)] \tag{12}$$

$$\frac{\partial f}{\partial \sigma_2} = s = 2\alpha\sigma_0^2 + \sigma_0\sigma_{90}[c + p + q - (pt + q\alpha t)]$$

In above equation,

$$\varepsilon_1^* = \frac{r^2 + \alpha rs}{r^2 + \alpha s^2}$$

$$\varepsilon_2^* = \frac{\alpha r^2 + rs}{r^2 + \alpha s^2} \tag{13}$$

For predicting negative strain range of FLD, Hill assumed that necking occurs in the rolling direction [3]. The proposed limit strains to predict the left side of FLD for different yield functions are shown in Eqs. (14) and (15).

$$\varepsilon_1^* = \frac{\left(\frac{\partial f}{\partial \sigma_1}\right)}{\left(\frac{\partial f}{\partial \sigma_1}\right) + \left(\frac{\partial f}{\partial \sigma_2}\right)} n$$

$$\varepsilon_2^* = \frac{\left(\frac{\partial f}{\partial \sigma_2}\right)}{\left(\frac{\partial f}{\partial \sigma_1}\right) + \left(\frac{\partial f}{\partial \sigma_2}\right)} n \tag{14}$$

Following equations express left side of forming limit diagram when using Hill's localized instability criterion.

$$\varepsilon_{l1} = \frac{1 + (1 - \alpha)R}{1 + \alpha} n$$

$$\varepsilon_{l2} = \frac{\alpha + (1 - \alpha)R}{1 + \alpha} n \tag{15}$$

2.3.2. NADDRG model

The North American Deep Drawing Research Group (NADDRG) proposed an empirical equation to calculate FLD which simplifies the theoretical prediction of FLDs [17]. In the introduced model, the FLD is composed of two lines which intersect the point in the plane strain region of FLD. The slopes of these lines are about 20 and 45 located on the right and left side of the forming limit diagram, respectively. The

proposed equation (Eq. 16) to calculate the limit strain would be expressed as follow:

$$\varepsilon_{10} = \frac{(23.3 + 14.13t)n}{0.21} \tag{16}$$

3   DESIGN OF THE EXPERIMENT

3.1. Tensile test

To omit edge effects associated with shearing processes, uni-axial tensile specimens were cut by wire EDM according to ASTM-E8 standard (Fig. 1). Due to the errors elimination resulted from misalignment of tensile specimens during tensile testing, at least two samples at each direction (0º, 45º and 90º) with respect to rolling directions were precisely cut. Tensile tests were carried out according to ASTM-E517-00 standard [18]. This standard deals with anisotropy of sheet materials as well as yield and tensile strength and the elongations in different directions with respect to rolling direction. During the tests, in addition to an extensometer, which monitors longitudinal elongations and the corresponding longitudinal strain, a strain gauge was used to monitor the width strain simultaneously. Consequently anisotropy of the sheet material could be obtained.

Tensile tests were carried out under constant strain rate of 1×10^{-3} S^{-1} at room temperature. After conducting the tensile test, the recorded tensile forces versus specimen's elongation were converted into true stress against true strain as well as engineering stress-strain curve.
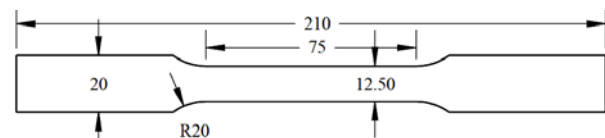
Fig. 1   Tensile test dimensions cut according to ASTM-E8 standard

Although R-value is introduced as the ratio of width strain to thickness strain, the thickness strain, ε_t, in thin sheets could not be accurately measured. Hence, by measuring longitudinal and width strains and also by implementing the principle of volume constancy (Eq. 17), the thickness strain (Eq. 18) can be presented as follows:

$$\varepsilon_l + \varepsilon_w + \varepsilon_t = 0 \tag{17}$$

$$\varepsilon_t = -\left(\varepsilon_l + \varepsilon_w\right) \tag{18}$$

For each direction, the strain ratio (R-value) was calculated. Subsequent to that, normal anisotropy as well as planar anisotropy was calculated according to the International Standard ASTM-E517-00 formulas. Equations (19) and (20) show how normal and planar anisotropy are obtained.

$$R_{(x)^\circ} = \frac{\varepsilon_{w(x)^\circ}}{\varepsilon_{t(x)^\circ}} \tag{19}$$

$$R = \frac{R_0 + 2R_{45} + R_{90}}{4}$$

$$\Delta R = \frac{R_0 + R_{90} - 2R_{45}}{2} \tag{20}$$

In the above equations, *R* is the normal and *ΔR* is the planar anisotropy.

4 FINITE ELEMENT APPROACH

In this paper, Auto form Master 4.4 as a very powerful tool to simulate sheet metal forming process, was employed for FE analysis of forming limit diagrams. As discussed before, tensile tests were carried out according to ASTM-E517-00 standard to obtain plastic behavior along with anisotropy of sheet materials. The properties were then introduced to the software as input material data.

For the approach, first CAD data were modeled in CATIA software and then were imported into Auto form environment. In order to cover full range of the FLD, different specimens with different groove dimensions were modeled to simulate the tension-compression side to tension-tension side of the FLD. The specimen dimensions are presented in Table 1.

Table 1 Dimensions of different FLD samples

	Sample #	A(mm)	B(mm)
	1	100	5
	2	100	12
	3	100	20
	4	100	30
	5	100	40
	6	100	50
	7	100	-
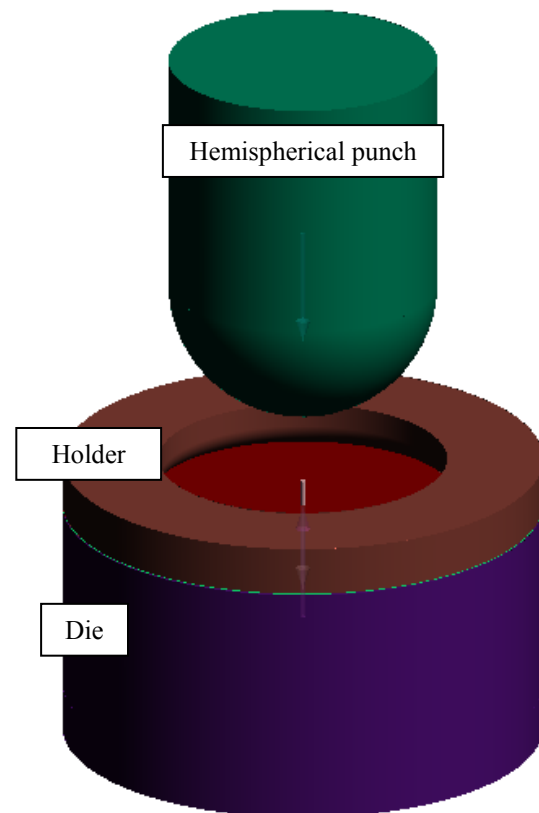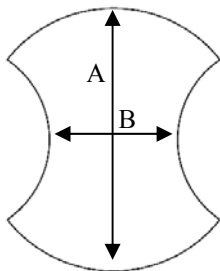
Fig. 2 Finite element modelling of pure stretching of samples with hemispherical punch in Auto form 4.4 software

For the FE simulation, the punch, holder and die considered as rigid parts. A displacement velocity of 1 mm/s was considered for the hemispherical punch while the clamping force was adjusted to 200 tons. Frictional coefficient was adjusted to 0.15 between the sheet surface and each contact surfaces. Major and minor strains were recorded precisely after each time step to evaluate the numerical FLD deduced from the simulations.
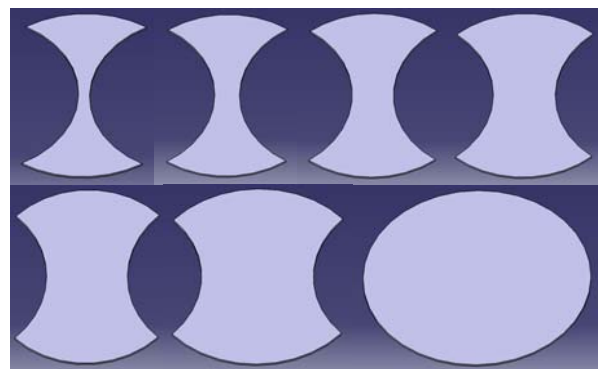
Fig. 3 Different samples with different shapes used for FE analysis

5   RESULTS AND DISCUSSION

5.1. Uni-axial tensile test

Tables 2 to 4 show experimentally determined mechanical properties for Ti-6Al-4V, AA7075-T6 and AA2024-T3 sheets, respectively. These mechanical properties are obtained from uni-axial tensile test. As it can be seen, for Ti-6Al-4V sheets, anisotropy coefficients are too high which poses the major reason that this alloy resists to thinning during the sheet metal forming processes. By comparing the work-hardening exponents between three aerospace materials, it can be deduced that although Ti-6Al-4V has n-values between those of 7075 and 2024 alloys, due to high normal anisotropy and resistance to thinning, higher formability is expected for this alloy.

AA7075-T6 sheets are somehow brittle due to T6 temper condition. The low work hardening values as well as small anisotropy coefficients prove that this alloy has very low formability, but high strength characteristics of T6 tempered have made this alloy suitable to be used in manufacturing of high-strength aerospace components. AA2024-T3 sheets as the other well-known aerospace alloy, have average formability in comparison with Ti-6Al-4V and AA7075-T6 sheets. AA2024-T3 is extensively used in manufacturing of wing tension members, shear webs, ribs and structural parts of aircrafts. The chief concern of this alloy specifications are high fatigue performance and fracture toughness which are combined with high strength to weight ratio.

5.2. Calculation of FLD

Figs. 4, 5 and 6 shows different yield surfaces for Ti-6Al-4V, AA2024-T3 and AA7075-T6 sheets, respectively. In Fig. 4, as it can be observed, calculated yield locus by using Von-Mises yield criterion covers less area in comparison with other yielding surfaces. In calculation of strain energy criterion, effect of anisotropy of material is not considered. Therefore, it is shown that by using Hill's 48 and Hill's 93 yield criteria, yield loci with larger surfaces would be attained. High normal anisotropy of Ti-6Al-4V sheets (R_{ave}>1), will cause the yielding surfaces to be extended along the biaxial stress axis. Effect of the yield surface on the forming limit curves will be discussed subsequently.

Figs. 5 and 6 show yield surface shapes for AA7075-T6 and AA2024-T3 sheets where the average R-value is smaller than 1. Average anisotropy deduced from uni-axial tension for these two alloys will cause the yielding surfaces to be decreased along the biaxial stress axis. Consequently, despite for alloys with average anisotropy more than 1 (R>1), the yield surface shape tends to extend along the biaxial stress axis; the yield surface of alloys with average anisotropy less than 1 (R<1) tend to decrease along the biaxial stress axis.

Table 2 Mechanical properties of 1.08mm Ti-6Al-4V sheets obtained from uni-axial tensile test

Parameters	Angle to rolling direction		
	0º	**45º**	**90º**
Density, (gr/cm³)	4.43	4.43	4.43
Poisson's ratio		0.342	
Yielding stress, (MPa)	544	558	571
Ultimate tensile stress, (MPa)	632	607	629
Total elongation, (%)	30.7	27.2	28
Anisotropy coefficient,	2.46	4.12	3.83
Normal anisotropy		3.63	
Strain hardening exponent	0.15	0.13	0.16
Strength coefficient, (MPa)	975	912	1022

Table 3 Mechanical properties of 0.78mm AA7075-T6 sheets obtained from uni-axial tensile test

Parameters	Angle to rolling direction		
	0º	**45º**	**90º**
Density, (gr/cm³)	2.8	2.8	2.8
Poisson's ratio		0.33	
Yielding stress, (MPa)	480	470	442
Ultimate tensile stress, (MPa)	543	538	537
Total elongation, (%)	13.5	13	11.1
Anisotropy coefficient	0.64	0.72	0.63
Normal anisotropy		0.6175	
Strain hardening exponent	0.1	0.1	0.11
Strength coefficient , (MPa)	760	755	739

Table 4 Mechanical properties of 0.3mm AA2024-T3 sheets obtained from uni-axial tensile test

Parameters	Angle to rolling direction		
	0º	**45º**	**90º**
Density, (gr/cm³)	2.8	2.8	2.8
Poisson's ratio		0.33	
Yielding stress, (MPa)	330	314	337
Ultimate tensile stress, (MPa)	417	403	431
Total elongation, (%)	20.3	18.1	19.7
Anisotropy coefficient	0.75	1.05	0.682
Normal anisotropy		0.88325	
Strain hardening exponent	0.16	0.15	0.16
Strength coefficient, (MPa)	590	572	585
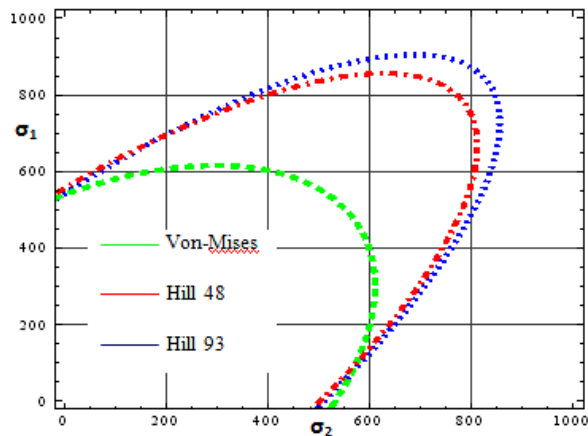
Fig. 4   Yield surface shape for Ti-6Al-4V
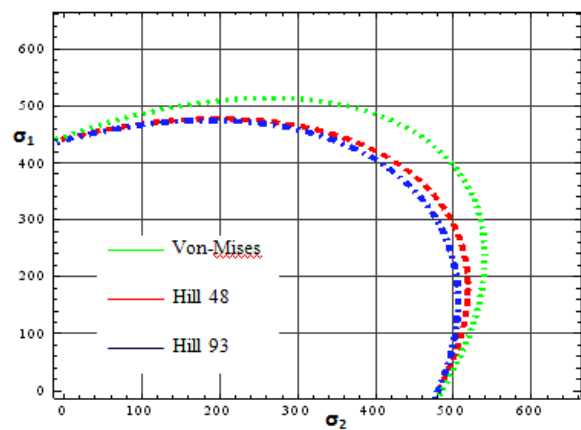
Fig. 5   Yield surface shape for AA7075-T6
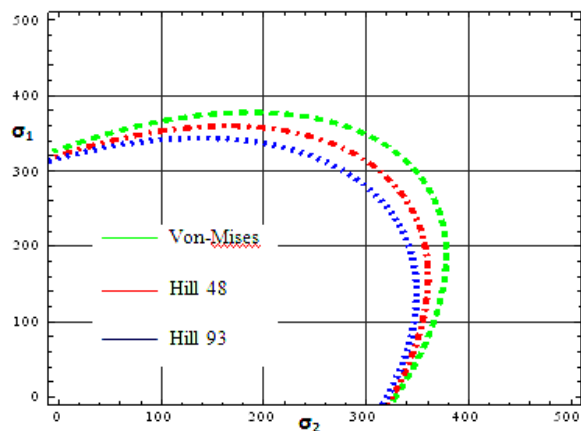
Fig. 6   Yield surface shape for AA2024-T3

Figs. 7, 8 and 9 show theoretical prediction and numerical calculation of forming limit diagrams for Ti-6Al-4V, AA7075-T6 and AA2024-T3 sheets, respectively. As shown in Fig. 7, calculated curves by using Hill's 48 and Hill's 93 localized instability

criteria lie in lower level than the curve calculated by using empirical equation proposed by NADDRG. The main reason for this would be inconsideration of anisotropy in empirical equation proposed by IDDRG. As it can be observed, for three sheet materials, Forming limits deduced from numerical simulation are in good agreement with the theoretical predictions when Hill93-Swift is the criterion.

There are two material properties which have more influence on forming limit diagram, the anisotropy and the work-hardening exponent. As discussed in the literature [19], R-values more less one (R<1), will result in reduction of limit strains in biaxial stretching and also lower levels for FLD in plane strain region are expected.

Hence, by using Hill's theories, which consider anisotropy of materials in FLD calculation, predicted limit strains are more realistic in comparison with FLDs predicted by using NADDRG equation. For Ti-6Al-4V, regarding to very high normal anisotropy (R>>1), the sheet material severely resists to thinning. Consequently, more limit strain ranges on the left side of FLD are attainable.

Second material property which directly influences the FLD is the work-hardening exponent (n-value). For most materials, forming limit curve intersects the major strain axis at the point equivalent to n-value. As n-value decreases, the limit strain level decreases. For Ti-6Al-4V, as discussed in previous sections, the work-hardening exponent obtained from tensile test is about 0.15. This consequences the major strain value at the range between 0.14 up to 0.16 considering Hill's yield criteria for FLD prediction.
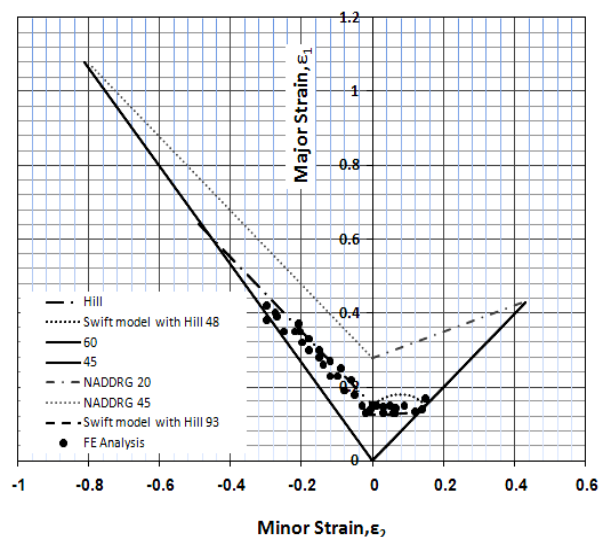
Fig. 7   Theoretical and numerical forming limit diagram for Ti-6Al-4V
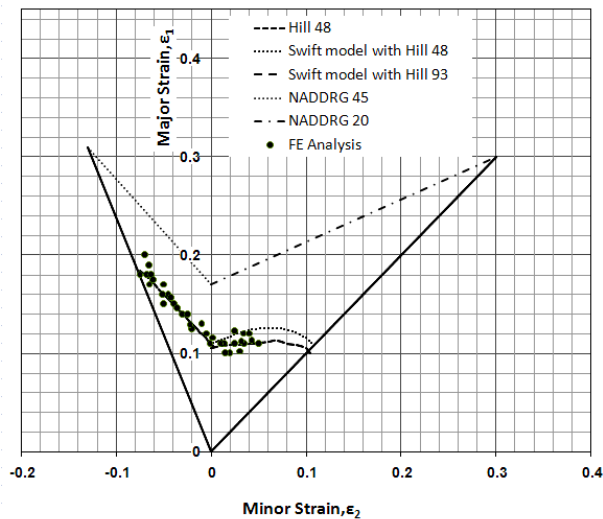
Fig. 8   Theoretical and numerical forming limit diagram
for AA7075-T6

In Fig. 7 it is also observed that forming limit curve
predicted by Swift model with Hill 48 on the right side
of the FLD, increases somewhat slowly and then
decreases when it becomes nearer to equi-biaxial stress
state, whereas by using Swift model with Hill 93, the
predicted FLD increases and decreases slower from
plane strain to equi-biaxial state of stress region.
Fig. 9 shows forming limit diagram calculated for
AA2024-T3 sheets. It is observed that due to smaller
anisotropy coefficients in comparison with Ti-6Al-4V,
this alloy has smaller forming limits at the left side of
the FLD. This fact shows that this alloy is not
resistance to thinning regarding to small R-values.
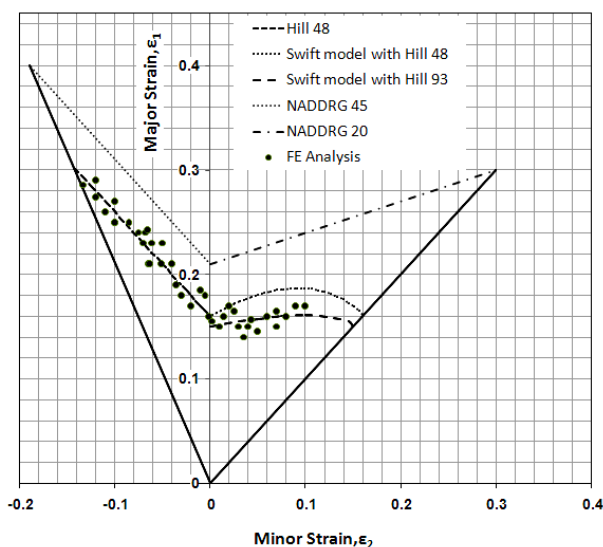
Fig. 9   Theoretical and numerical forming limit diagram
for AA2024-T3
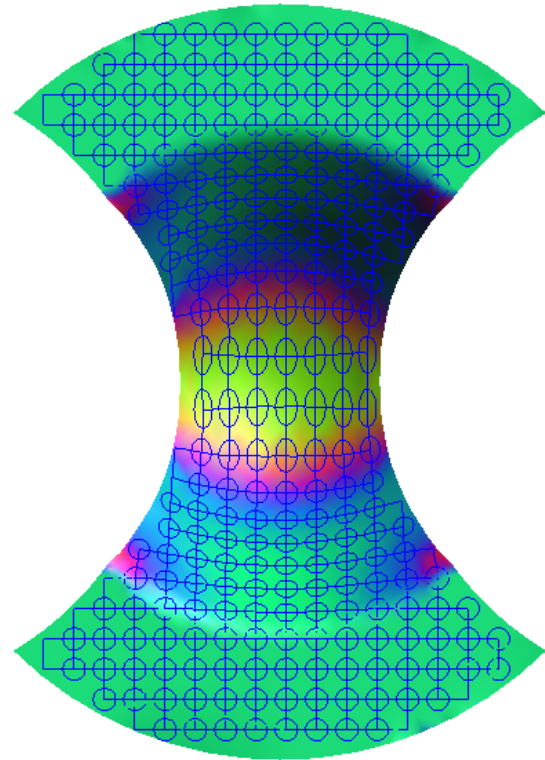
Fig. 10   Finite element simulation of samples in Auto form
software (Sample #3)

In the FE software, as mentioned before, all the
samples were engraved with a grid pattern of 3 mm
circles. The major and minor strains were then
measured from the deformed circles. Fig. 10 shows
sample #3 which is covered with deformed and non-
deformed circles.

6   CONCLUSION

In the present study, formability of 1.08 mm Ti-6Al-4V
titanium sheet alloys as well as 0.78 mm AA7075-T6 and
0.3 mm AA2024-T3 aluminum sheet alloys were
investigated through uni-axial tensile test, theoretical
calculations and numerical simulations. For uni-axial
tensile test, tensile specimens were cut according to
ASTM-E8 in different angles in relation to rolling
direction and then were tested according to ASTM-E517-
00 standard to obtain anisotropy coefficients along
different directions.
Several yield functions were used to investigate the yield
surface shapes for Ti-6Al-4V, AA2024-T3 and AA7075-
T6 sheets. Theoretical calculation of forming limit curves
were carried out by using empirical model proposed by
NADDRG and different Hill-Swift models. These curves
were then compared with the FLDs deduced from

numerical simulations of different-shaped specimens in a powerful FE tool. Based upon experimental and numerical results, the following conclusions are drawn:

1. Ti-6Al-4V titanium sheet alloys have high normal anisotropy as well as planar isotropy which pose the main reason that this alloy resists to thinning during the deformation.

2. Two material constants (work-hardening exponent and anisotropy coefficient) have significant influence on forming limit curve. Forming limit diagram decreases when work-hardening exponent decreases. Smaller values of anisotropy will also result in lower level of FLD.

3. AA7075-T6 sheets have very low formability due to artificially aged condition (T6-tempered) which result in lower n-values along with lower R-values. Forming limits for this alloy stand in very low levels. As a result, in order to successfully produce an aircraft component made from this alloy, novel processes such as hydroforming should be applied.

4. AA2024-T3 sheets have average formability when compared to two other alloys investigated in this paper. The forming limit region for this alloy is almost equal in both sides of the FLD.

Nomenclature	Description
$\sigma_1, \sigma_2, \sigma_3$	Principle stress
σ_b	Biaxial yield stress
Y	Yield stress
$\sigma_x, \sigma_y, \sigma_z, \tau_{xy}, \tau_{xz}, \tau_{yz}$	Stress components
$f(\sigma_{ij})$	Yield function
F, G, H, L, M, N	Coefficients of Hill'48 yield criterion
$r_{11}, r_{22}, r_{33}, r_{12}, r_{13}, r_{23}$	Yield stress ratios in Hill'48 yield criterion
R_0, R_{45}, R_{90}	Anisotropy coefficients
R	Normal anisotropy
ΔR	Planar anisotropy
c, p, q	Coefficients of Hill'93 yield criterion
ε_1^*	Major limit strain on right side of FLD
ε_2^*	Major limit strain on right side of FLD
α	Stress ratio
ε_{l1}	Major limit strain on left side of FLD
ε_{l2}	Minor limit strain on left side of FLD
$\varepsilon_l, \varepsilon_w, \varepsilon_t$	Strains at longitudinal, width and thickness direction

REFERENCES

[1] Keeler, S. P., "Circular grid systems: A valuable aid for evaluation sheet forming", Sheet Met. Ind., Vol. 45, 1969, pp. 633-640.

[2] Goodwin, G. M., "Application of strain analysis to sheet metal forming problems", Metall. Ital., Vol. 60, 1968, pp. 767-771.

[3] Hill, R., "On discontinuous plastic states, with special reference to localized necking in thin sheets", Journal of the Mechanics and Physics, Vol. 1, 1952, pp. 19-30.

[4] Swift, H. W., "Plastic instability under plane stress, Journal of the Mechanics and Physics of Solids 1, 1952, pp. 1-18.

[5] Marciniak, z., Kuczynski, K., "Limit strains in the processes of stretch-forming sheet metal", Int. Journal Mech. Sci., Vol. 9, 1967, pp. 609-620.

[6] Marciniak, Z., Kuczynski, K., and Pokora, T., "Influence of the plastic properties of material on the forming limit diagram for sheet metal in tension", Int. Journal Mech. Sci., Vol. 15, 1973, pp. 789-805.

[7] Banabic, D., Valasutean, S., "The effect of vibratory straining upon forming limit diagrams", Journal Mater. Process. Technol., Vol. 34, 1992, pp. 431-437.

[8] Banabic, D., Dorr, I. R., "Prediction of the forming limit diagrams in pulsatory straining", Journal Mater. Process. Technol., Vol. 45, 1-4, 1994, pp. 551-556.

[9] Hutchinson, J. W., Neale, K. W., "Sheet necking: I. Validity of plane stress assumptions of the long wavelength approximation", in: D.P. Koistinen, N. M. Wang (Eds.), Mechanics of Sheet Metal Forming, Plenum Press, New York, 1978, pp. 111-126.

[10] Barata Da Rocha, A., Jalinier, J. M., "The development of strain gradients in sheet metal forming processes", in: Proc. Int. Symp. Plastic Instability, Paris, France, 1983, pp. 35-47.

[11] Laukonis, J. V., Ghosh, A. K., "Effects of strain path changes on the formability of sheet metals", Metall. Trans. A 9, 1978, pp. 1849-1856.

[12] Lian, J., Baudelet, B., "Forming limit diagram of sheet metal in the negative minor strain region", Mater. Sci. Eng. 86, 1987, pp. 137-144.

[13] Marciniak, Z., Kuczynski, K., "Limit strains in the processes of stretch-forming sheet metal", Int. J. Mech. Sci., Vol. 9, 1967, pp. 609-620.

[14] Hill, R., "A theory of the yielding and plastic flow of anisotropic metals", Proceedings of the Royal Society of London A, Vol. 193, 1948, pp. 197-281.

[15] Hill, R., "A user-friendly theory of orthotropic plasticity in sheet metals", International Journal of Mechanical Sciences, Vol. 35, No. 1, 1993, pp. 19-25.

[16] Banabic, D., "Limit strains in the sheet metals by using the new Hill's yield criterion (1993), Journal of Materials Processing Technology, Vol. 92-93, 1999, pp. 429-432.

[17]   Levy, S. B., "A comparison of empirical forming limitcurves for low carbon steel with theoretical forming limit curves of Ramaekers and Bongaerts", IDDRG WG3, Ungarn, 13-14 June, 1996.

[18]   ASTM Committee E28/Subcommittee E28.02, 2006. Standard Test Method for Plastic Strain Ratio r for Sheet Metal, ASTM E517-00.

[19]   Djavanroodi, F., Derogar, A., "Experimental and numerical evaluation of forming limit diagram for Ti-6Al-4V titanium and Al6061-T6 aluminum alloys sheets", Int. J. Materials & Design, Vol. 31, 2010, pp. 4866-4875.